Supplementary Information

Engineering an Artificial Flavoprotein Magnetosensor.

Chris Bialas,[1‡] Lauren E. Jarocha,[2‡] Kevin B. Henbest,[3] Tilo M. Zollitsch,[2] Goutham Kodali,[1] Christiane R. Timmel,[3] Stuart R. Mackenzie,[2] P. Leslie Dutton,[1] Christopher C. Moser,*[,1] and P. J. Hore*[,2]

1. Johnson Research Foundation, Department of Biochemistry and Biophysics, University of Pennsylvania, Philadelphia, PA 19104, U.S.A.

2. Department of Chemistry, University of Oxford, Physical and Theoretical Chemistry Laboratory, OX1 3QZ, United Kingdom

3. Department of Chemistry, University of Oxford, Inorganic Chemistry Laboratory, OX1 3QR, United Kingdom

Table of Contents

Materials and Methods

Unless otherwise noted, all of the reagents were commercially available from Fischer Scientific or Sigma Aldrich.

Protein expression and purification

The original design first described in Farid *et al.* (2013) was constructed as a synthetic gene from DNA2.0 in a PJ414 vector.[1] All designs were generated using PCR mutagenesis from this parent vector. Mutagenesis was carried out using AccuPrime™ Pfx SuperMix (Invitrogen). A volume of 22.5 µL of AccuPrime™ Pfx SuperMix was combined with 1 µL of solution containing 100 ng of parent DNA, 0.5 µL of a 100 µM solution of each primer and 2.7 µL of MasterAmp PCR Enhancer. The sample was cycled on an Eppendorf Master Cycler Pro (model 6321) using the following procedure: initial denaturation at 95 °C for 5 minutes, followed by repeating a cycle of denaturation at 95 °C for 15 seconds, annealing at 65 °C for 30 seconds, and extension at 68 °C for 5 minutes for a total of 18 times. A final extension was done at 68 °C for 5 minutes and ended with a hold at 4 °C. Samples were then digested with 0.5 µL of Dpn-1 (New England Biolabs) for 1 hour at 37 °C. A volume of 1 µL of this DNA was transformed into DH5 α cells (Genechoice Genesee Scientific) and grown overnight on an LB agar ampicillin plate (75 mg/ml) at 37 °C. The following day, four single colonies were picked and outgrown in LB media with ampicillin and their DNA was extracted using a Miniprep Kit (Qiagen). The sequence was verified at the University of Pennsylvania DNA sequencing Core Facility using a T7 promoter primer.

All constructs were designed with a six-histidine tag separated by a TEV cleavage site (Scheme S1). All were expressed in *E. coli* BL21 (DE3) cells (Genechoice Genesee Scientific). Two liter cultures of TB media where grown to OD_{600} 0.7-0.8 at 37 °C, followed by a 5-hour induction with 1 mM IPTG. The cells were harvested by centrifugation (10000 RPM, 5 minutes) and stored at 20 °C until use. Cells were thawed and suspended in Ni Wash buffer (20 mM NaH_2PO_4, 0.5 M NaCl, 10 mM imidazole, pH 8.0) with 1% OTG, then homogenized and lysed by sonication in a bath sonicator. The lysate was centrifuged (25,000*g*, 35 min) and the supernatant applied to a NiNTA superflow resin (Qiagen) on an Akta Fast protein liquid chromatography (FPLC) system. The fusion protein was eluted using Ni Elution buffer (20 mM NaH_2PO_4, 0.5 M NaCl, 250 mM imidazole, pH 8.0), and cleaved by recombinant tobacco etch virus N1a(TEV) protease overnight at room temperature in Ni Elution buffer supplemented with 1 mM TCEP (reductant) and 0.5 mM EDTA. The sample was dialyzed into Ni Wash buffer, and applied to the NiNTA column with the flow through and wash collected. The sample was then concentrated to about 15 mL using a stirred cell (Amicon model 8050) equipped with a 10,000 MWC filter. The sample was flash frozen in liquid nitrogen and stored at −20 °C until use.

Flavination of the maquettes

The protein was flavinated using an optimized version of a protocol first described in Farid *et al*. *(*2013).[1] A typical 5 mL reaction contained concentrated maquette (a few hundred millimolar, in Ni Wash), a 3-5 molar excess of 8-bromoriboflavin (in DMF, final DMF concentration not to exceed 20%), and TCEP at a final concentration of 1.25 mM. The pH of the solution was adjusted to 9.0 with NaOH, and stirred overnight at 50 °C while protected from light. The sample was purified on a Waters reverse-phase HPLC (C18 column Gracie, H_2O + 0.1% TFA aqueous phase and acetonitrile +

0.1% TFA organic phase), flash frozen in liquid nitrogen and lyophilized (Figure S1). Flavination was verified by the presence of a 475 nm band on the HPLC detector as well as by ESI, matrix assisted laser desorption ionization mass spectrometry.

Matrix assisted laser desorption ionization mass spectrometry

Samples were either taken directly from the HPLC or, if they had been lyophilized, dissolved in 66% acetonitrile, 44% water + 0.1% TFA. A sample volume of 1 µL was mixed with 1 µL of saturated matrix solution (sinapinic acid in TFA) and spotted on a sample target. The target was then dried under vacuum and measurements taken in linear flight mode (Figure S2).

Spectroscopic characterization

The sample was dissolved in redox buffer (20 mM KH_2PO_4, 100 mM KCl, pH 7.4). All measurements were in this buffer unless otherwise stated.

UV-visible spectra (Figure 2, Figure S4) were collected in a quartz cuvette (1 mL, 1 cm path) with a Varian Cary-50 spectrophotometer at room temperature. The presence of a band at 475 nm indicated incorporation of the flavin under normal (oxidizing) conditions. UV-visible spectra used to monitor photodegradation and concentration prior to transient absorption experiments were collected with a Varian Cary-60 spectrometer, using a small volume quartz cuvette (1 cm path length, 200 µL volume) at room temperature.

Secondary structure was monitored by CD spectroscopy (Aviv Model 410) with a quartz cuvette (400 µL, 1 mm path) from 200 nm to 300 nm at 25 °C (Figure S3A). The thermal stability was determined by monitoring the ellipticity at 222 nm every 2 °C from 2 °C to 98 °C (Figure S3B). The melting temperatures were calculated using a single term Boltzmann fit. Typical concentration was 20-30 µM.

Steady state fluorescence data (Table 1 and Figure S5) where analysed in a quartz fluorescence cuvette (1 ml, 1 cm path) on a Horiba Fluorolog 2 spectrophotometer at 20 °C. All spectra where corrected for fluctuations in lamp intensity. Typical concentrations were 3-5 µM (OD_{475} 0.05-0.1). Quantum yield measurements were made by integrating the area under the curve of the steady state spectrum relative a riboflavin standard (Φ = 0.267)[2] and correcting for concentration and extinction.

Fluorescence lifetimes where determined using a time-correlated single photon counting (TCSPC) spectrometer at the Ultrafast Optical Processes Laboratory at the University of Pennsylvania. Samples were prepared in redox buffer at approximately 5 µm (OD_{475} = 0.1) at room temperature in a quartz cuvette (1 mL, 1 cm path). A 482 nm picosecond diode laser (PicoQuant GmbH; Berlin, Germany) was used as an excitation source. Emission was recorded at 512 nm on a Becker-Hickl TCSPC board and analysed with FluoFit software (Picoquant). The best fit was a triple exponential (Figure S6). All spectra where corrected for fluctuations in lamp intensity.

The steady state phosphorescence spectrum (Figure 2) was recorded on an Edinburgh Instruments FS 920 Fluorimeter equipped with a liquid nitrogen dewar. A sample volume of 200 µM was flash frozen in a glass tube and spectra taken at liquid nitrogen temperatures.

Electrochemical characterization

Redox titrations (Table 1, Figure S7A) were performed to determine the redox potential of the flavin using a spectroelectrochemical system. A typical sample contained 10-30 μM protein and the following redox mediators: duroquinone (10 μM), pyocyanin (10 μM), 2-hydroxy-1,4-naphthoquinone (10 μM), phenazine (10 μM), anthraquinone-2-sulfonate (20 μM), benzyl viologen (10 μM), and methyl viologen (10 μM). The potential of the solution was modulated from 0 mV to –500 mV vs. S.H.E. using a CH Instruments model 600C electrochemical analyser equipped with a Pine Instruments gold honeycomb electrode. The electrode was coated to prevent protein build-up by soaking in 2 mM cystamine for 45 minutes. The oxidation state of the system was monitored spectroscopically using an Ocean Optics DH-2000-BAL light source and a fiber-optic-guided USB 4000 diode array detector. The change from oxidized to reduced was monitored by the depletion in absorbance of the S1 band region of the flavin (475 nm). The data were then fitted to a Nernst equation (Eq. 1), where E_{cell} is the redox potential of the spectrochemical cell, E_m is the redox potential of the flavin, n is the number of electrons transferred and [ox, red] is the concentration of oxidized or reduced species present at a particular E_{cell}.

$$E_{cell} = E_m + \left(\frac{0.059}{n}\right)\log\left(\frac{[ox]}{[red]}\right) \quad (1)$$

At the redox potential (E_m), we saw no evidence of any semiquinone absorption, indicating an unstable flavin semiquinone and $n = 2$ was used for the fit.

Square wave voltammetry was used to record the midpoint potential of the TrpH/TrpH$^{\bullet+}$ redox couple (Table 1, Figure S7B). A gold electrode was sonicated in an Alconox solution for 5 minutes in a bath sonicator followed by polishing with alumina slurry (20 nm) for 1 minute in a figure of eight motion. The electrode was then rinsed, and sonicated for 5 minutes in distilled water. Electrochemical cleaning was performed in 0.5 mM sulfuric acid from –0.375 to 1.8 V for 50 cycles using a CH Instruments model 600C electrochemical analyser. The electrode was again rinsed with distilled water, then DMSO, and coupled to dithiobis(succinimidyl propionate) (DSP, Lomant's Reagent) in DMSO (4 mg/mL) for 30 minutes. The electrode was dipped into a concentrated protein solution in redox buffer (100 μL) for 2 hours to couple it to the DSP-bound electrode. The electrode was placed into a cell containing redox buffer and equipped with a Pt counter electrode and an Ag/AgCl reference electrode. The potential was swept from 0.7 V to 1.2 V vs. S.H.E. with a frequency of 300 Hz and a 25 mV step size. Each data point was the average of five separate scans. The background current due to the gold electrode was subtracted out in post-processing.

Electron transfer rate calculations

Predicted electron transfer rates were calculated using the Moser-Dutton Ruler (see below, Eq. (1)), an empirical expression that relates the rate of electron transfer in proteins to the edge-to-edge distance between donor and acceptor (*R*, in Angstroms), the driving force of the transfer (ΔG) and the reorganization energy (λ). The distance in the flavomaquettes is a rough estimate determined using the distance between the β carbon of the ligating cysteine and the Trp. Each helical turn was approximately 5.6 Å. It should be noted that these distances are obtained from a

model of general protein structure and do not take into account any conformational flexibility that may be present for the relevant cofactors. The driving force was calculated as the difference between the excited state of the flavin singlet or triplet (calculated from the S_0 or T_0 emission wavelength, respectively), and the redox potential of the reduced flavin and oxidized Trp radical (determined in this work). The reorganization energy is difficult to determine experimentally and a medium-to-large value was estimated for small polar maquettes. Therefore, these rates are strictly used as a rough estimate for the relative timescales and behaviour expected in the flavomaquettes. For a more complete discussion of reorganization energy and estimation in the Moser-Dutton Ruler see Moser *et al*. (2010).[3]

$$\log K_{\mathrm{ET}} = 13 - 0.6\left(R - 3.6\right) - 3.1\left(\Delta G + \lambda\right)^2 / \lambda \qquad (2)$$

General ΔG calculations

ΔG = (Redox Potential F/$F^{\bullet -}$ + Photon Energy) – (Redox Potential TrpH/ $TrpH^{\bullet +}$)

Specific ΔG values

ΔG(Singlet Electron Transfer) = -1.21 V

ΔG(Singlet Charge Recombination) = -1.2 V

ΔG(Triplet Electron Transfer) = -0.81 V

ΔG(Triplet Charge Recombination) = -1.2 V

Reorganization Energy

λ = 1.2 V

Table S1. Singlet electron transfer and charge recombination rate constants

		Forward Electron Transfer		Charge Recombination	
Design	**Distance (Å)**	**$\log(k_{ET}/s^{-1})$**	**k_{ET}/s^{-1}**	**$\log(k_{CR}/s^{-1})$**	**k_{CR}/s^{-1}**
W 13	5.6	11.8	6.31×10^{11}	11.8	6.31×10^{11}
W 16	11.2	8.44	2.75×10^{8}	8.44	2.75×10^{8}
W 20	16.8	5.08	1.20×10^{5}	5.08	1.20×10^{5}

Table S2. Triplet electron transfer and charge recombination rate constants

		Forward Electron Transfer		Charge Recombination	
Design	**Distance (Å)**	**log(k_{ET}/s^{-1})**	**k_{ET}/s^{-1}**	**log(k_{CR}/s^{-1})**	**k_{CR}/s^{-1}**
W 13	5.6	11.4	2.55×10^{11}	11.8	6.31×10^{11}
W 16	11.2	8.05	1.11×10^{8}	8.44	2.75×10^{8}
W 20	16.8	4.69	2.86×10^{4}	5.08	1.20×10^{5}

It is important to note that charge recombination rates calculated for the triplet electron transfer *only take into account the energetic considerations* for the charge recombination and neglect the fact that recombination is *spin forbidden for triplet radical pairs*.

Transient absorption and magnetic field effect measurements

The transient absorption spectrometer used to characterize maquette photochemistry and measure the magnetic field effect has been described elsewhere.[4] Briefly, 250 µL of sample is placed in a quartz cuvette (Hellma 104.002F QS, 10 mm path length, internal dimensions 2 × 10 × 45 mm) in the center of a cryostat (Oxford Instruments, Optistat CF) with the temperature controlled at 25.0 ± 0.1 K. Magnetic field pulses of approximately 4 ms duration were synchronized with the laser flash and generated using home-built Helmholtz coils. The maximum field at the position of the sample is 20 mT. Data were collected by alternating measurements with the magnetic field on and off.

Maquettes were prepared in redox buffer to a concentration of approximately 30 µM. Dissolution of the maquette resulted in a drop of the solution pH to a value of between 6.8 and 7.0 when starting with a phosphate solution at pH 7.4. Samples were centrifuged to remove any aggregates for 15 minutes at 9000 RPM and 4 °C and then measured by UV-visible spectroscopy.

Radical pairs were generated by flash photolysis using a Sirah Cobra dye laser pumped by a Continuum Surelite I Nd:YAG laser. Excitation was 5-7 mJ at 450 nm using Coumarin 460 as the dye in analytical grade methanol (Fischer Scientific). The repetition rate for data collection was 1 Hz for W13 and W16. This repetition rate was reduced for W20 and the control, where a 1-2 minute delay between shots was necessary to avoid complications caused by photoproduct formation (Figure S8, S9). Probe light was provided by a 1000 W xenon arc lamp (Oriel) passed through water and long pass filters to minimize exposure of the sample to unwanted wavelengths. The probe beam was set perpendicular to the pump excitation. Both pump and probe beams were controlled by mechanical shutters to reduce photodegradation of the samples. The transient absorption signal was detected using a monochromater (Oriel 77250) and photomultiplier tube (Hamamatsu R928) connected to an oscilloscope (LeCroy Waverunner LT342L). Data were transferred to a computer and analysed using Igor Pro (Wavemetrics Inc.) software.

Photoproduct characterization

During the course of spectroscopic characterization, an absorption band at 400 nm began to appear concurrently with the disappearance of the 475 nm feature. We attributed this to photodamage of the flavin. To identify this product, a 10 µM sample of flavin in redox buffer was deoxygenated by exchanging the atmosphere with high purity argon (Airgas) passed through a Vd scrubbing system for 30 minutes under stirring and illuminated for 1 hour. The sample was then studied using mass spectrometry and fluorescence spectroscopy (Figures S8, S9). From the data it was concluded that the major degradation product was maquettes-coupled lumichrome, consistent with known photodegradation pathways of free flavins in solution.[5]

Control

MHHHHHHGGDGGTENLYFQG

1. EIQKQFEDALQKFEEALNQFEDLKQL
   GGSGSGSGG
2. EIQKQFEDCLQKFEEALNQFEDLKQL
   GGSGSGSGG
3. EIQKQFEDALQKFEEALNQFEDLKQL
   GGSGSGSGG
4. EIQKQFEDALQKFEEALNQFEDLKQL

W16

1. GEIQKQFEDALQKFEEALNQFEDLKQL
   GGSGSGSGG
2. EIQKQFEDCLQKFEEWLNQFEDLKQL
   GGSGSGSGG
3. EIQKQFEDALQKFEEALNQFEDLKQL
   GGSGSGSGG
4. EIQKQFEDALQKFEEALNQFEDLKQL

W13

1. GEIQKQFEDALQKFEEALNQFEDLKQL
   GGSGSGSGG
2. EIQKQFEDCLQKWEEALNQFEDLKQL
   GGSGSGSGG
3. EIQKQFEDALQKFEEALNQFEDLKQL
   GGSGSGSGG
4. EIQKQFEDALQKFEEALNQFEDLKQL

W20

1. GEIQKQFEDALQKFEEALNQFEDLKQL
   GGSGSGSGG
2. EIQKQFEDCLQKFEEALNQWEDLKQL
   GGSGSGSGG
3. EIQKQFEDALQKFEEALNQFEDLKQL
   GGSGSGSGG
4. EIQKQFEDALQKFEEALNQFEDLKQL

Scheme S1. The amino acid sequences of all of the designs. The control maquette is shown with its upstream tag sequence: the start methionine (red), six-histidine tag (green), linker (light blue) and TEV site (purple) are highlighted in color. The helices and loops, which consist only of Gly and Ser residues, are shown on separate lines from the N to C terminus, and numbered in the same order they appear in the sequence. The flavin-binding cysteine (helix 2, position 9) is shown in orange and the tryptophan in blue on helix 2.

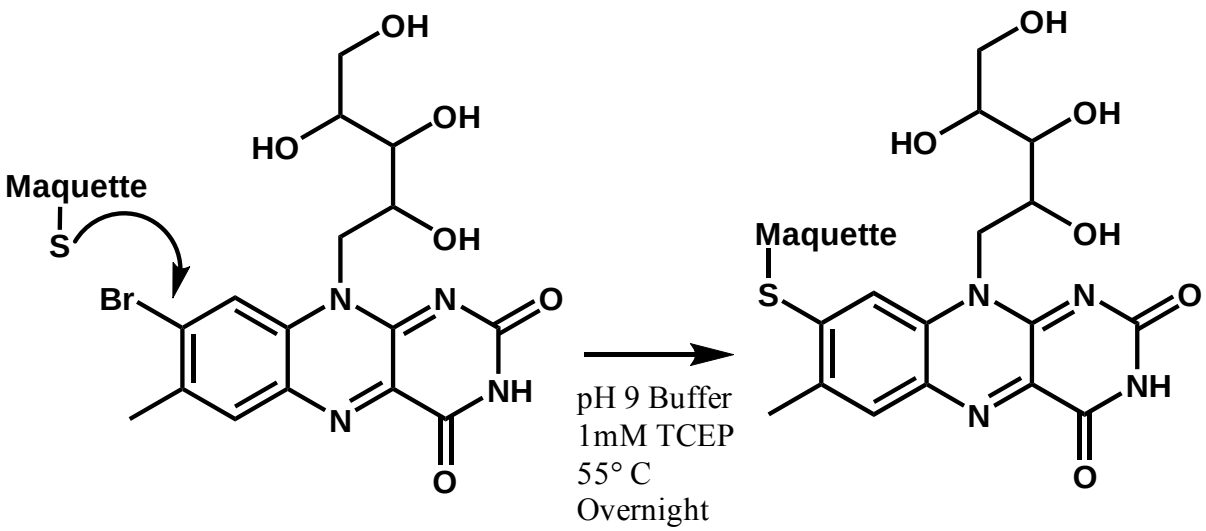

Scheme S2. The covalent attachment of 8-Br-riboflavin to a cysteine in the maquette. The reaction is performed in a high-pH buffer to ensure cysteine deprotonation and protected from light. TCEP is included to reduce inter-maquette disulphide bonds. Thiol based reductants are avoided to prevent side reactions with the flavin.

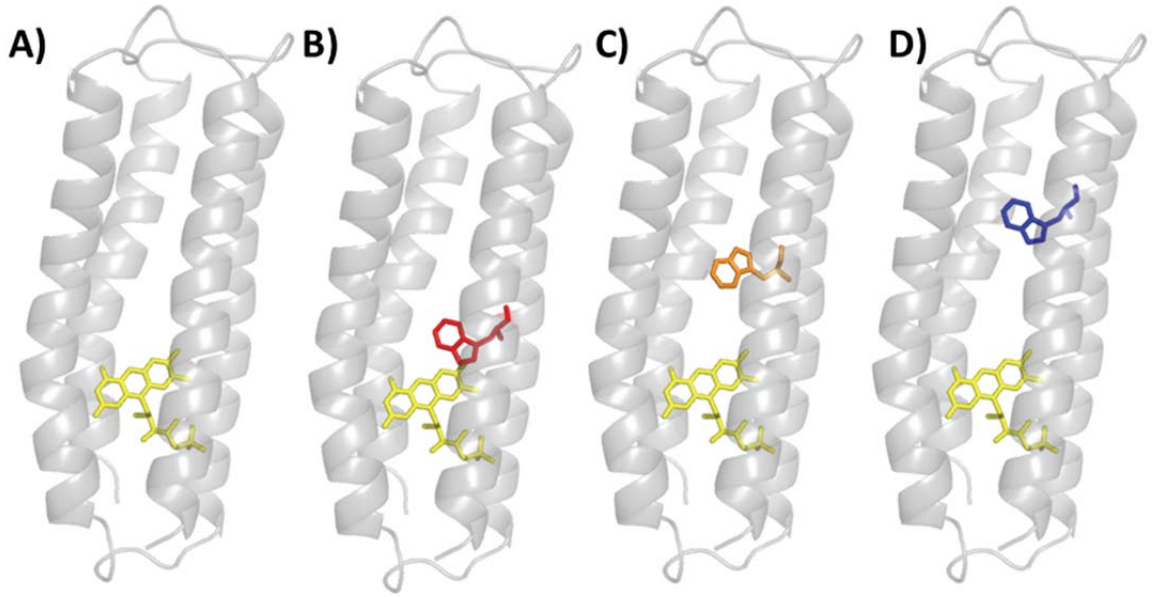

Figure S1. A representation of the four maquette designs used in these studies: A) the flavin-only control, B) W13 with the Trp one helical turn away from the flavin, C) W16 with the Trp two helical turns away from the flavin, and D) W20 with the Trp three helical turns away from the flavin.

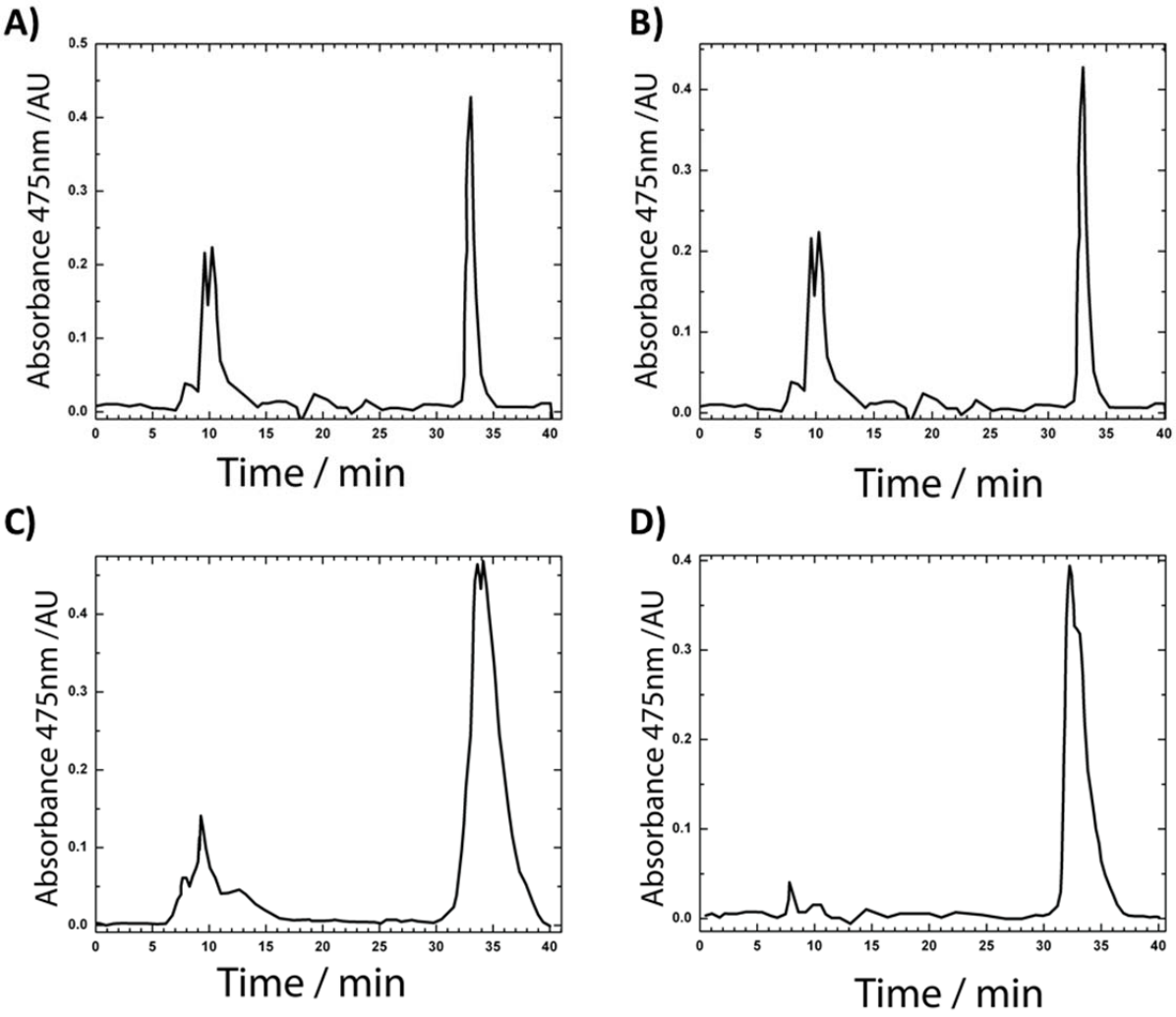

Figure S2. Reverse-phase HPLC traces of flavomaquettes: control (A), W13 (B), W16 (C) and W20 (D) taken at 475 nm. The sample was purified on a Waters reverse-phase HPLC (C18 column Gracie, H_2O + 0.1 % TFA aqueous phase and acetonitrile + 0.1% TFA organic phase). A 20-70% linear gradient of acetonitrile was used over 50 minutes to elute the protein at approximately 31 minutes. Injection peaks are present at approximately 10 minutes.

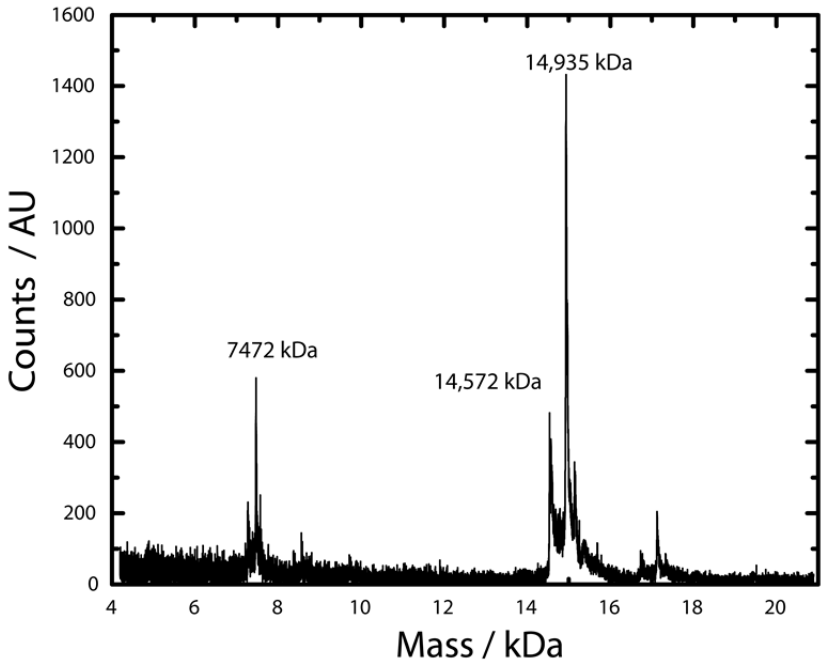

Figure S3. MALDI-TOF mass spectra of the control flavomaquette. The apo-protein appears at 14572 *m*/*z*, while the flavinated protein appears at 14935 *m*/*z*, 363 mass units higher, confirming the covalent attachment of the flavin.

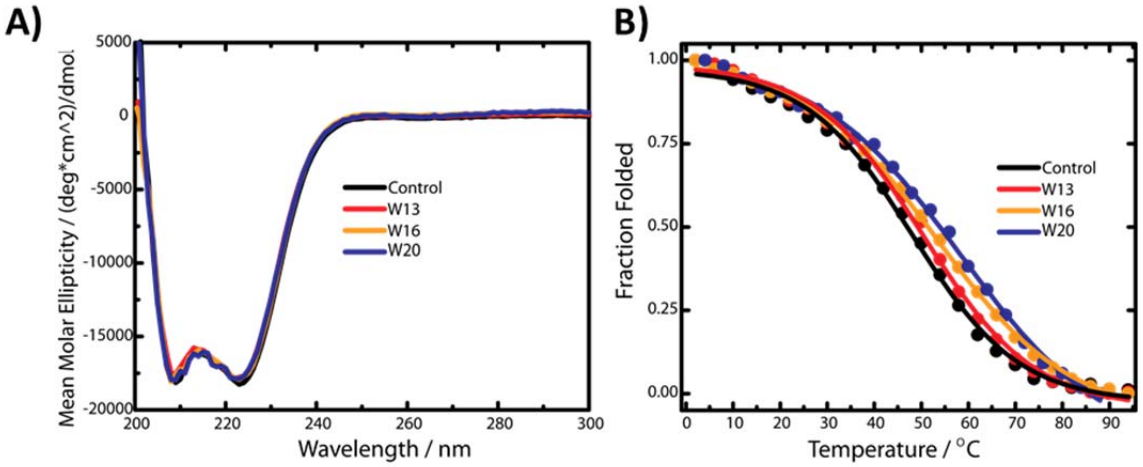

Figure S4. A) CD traces of the flavomaquettes with Trp residues at position W13, W16, and W20. The relative intensities at 208 nm and 222 nm suggest the maquette protein structure consists primarily of an α-helical bundle. B) Thermal stability curves of various flavomaquette designs. The T_m for each maquette is determined by monitoring the loss of helicity at 222 nm and fitting to a single Boltzmann distribution; control (black) 49 °C, W13 (red) 50.5 °C, W16 (orange) 53.2 °C and W20 (blue) 58.3 °C.

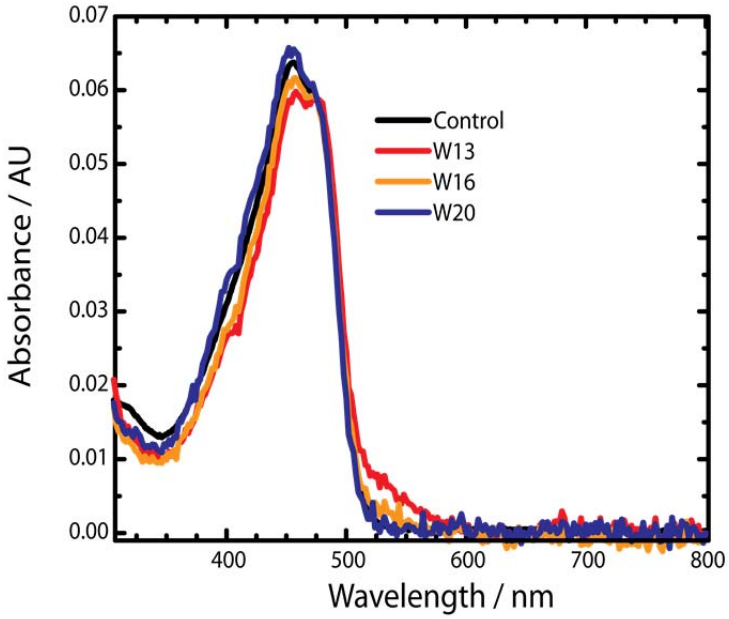

Figure S5. A comparison of the UV-visible spectra of the flavomaquette designs. The shoulder around 525 nm suggests a charge transfer band that increases as the flavin and Trp distance decreases.

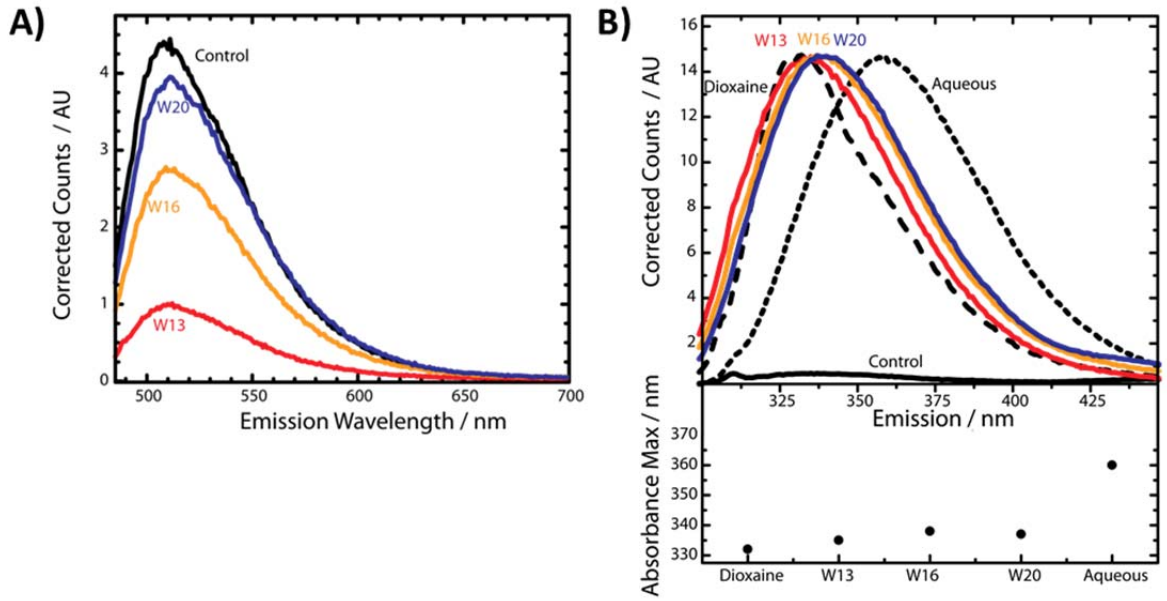

Figure S6. A) Steady state fluorescence of the flavin incorporated in the maquettes with varying flavin-Trp distances. B) A comparison of the normalized Trp fluorescence of the flavomaquette series. Free Trp in dioxane and an aqueous buffer are used as solvatochromic standards. The maximum of the Trp fluorescence in all the maquettes is blue-shifted relative to the aqueous standard, consistent with the Trp being located in the hydrophobic interior of the maquette α-helical bundle.

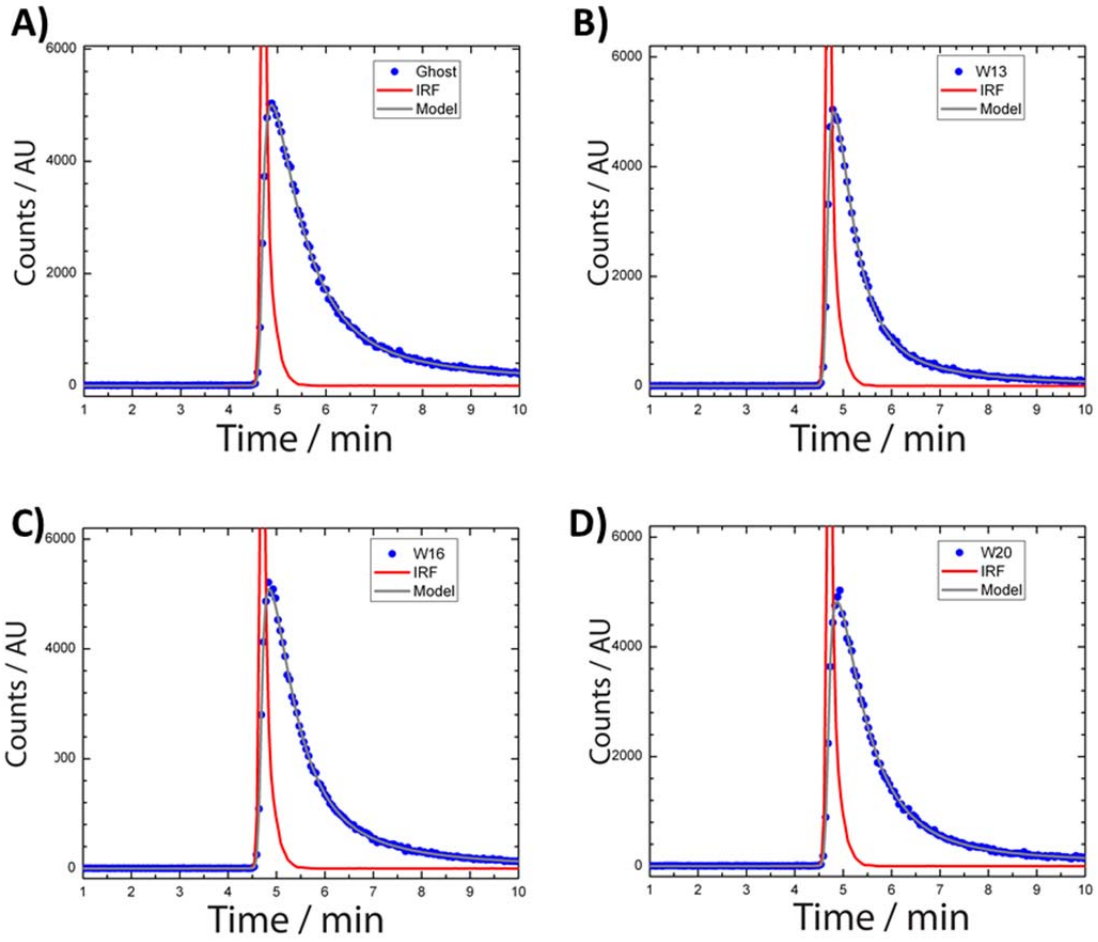

Figure S7. Time-correlated single photon counting decay curves (blue) and instrument response time functions (red) for A) the control, B) W13, C) W16, and D) W20. A 482 nm picosecond diode laser (PicoQuant GMbH) was used as an excitation source. Emission was recorded at 512 nm on a Becker-Hickl TCSPC board. The best fit to the data was triple exponential, and the average fluorescence lifetime calculated from the amplitude average is reported in Table 1.

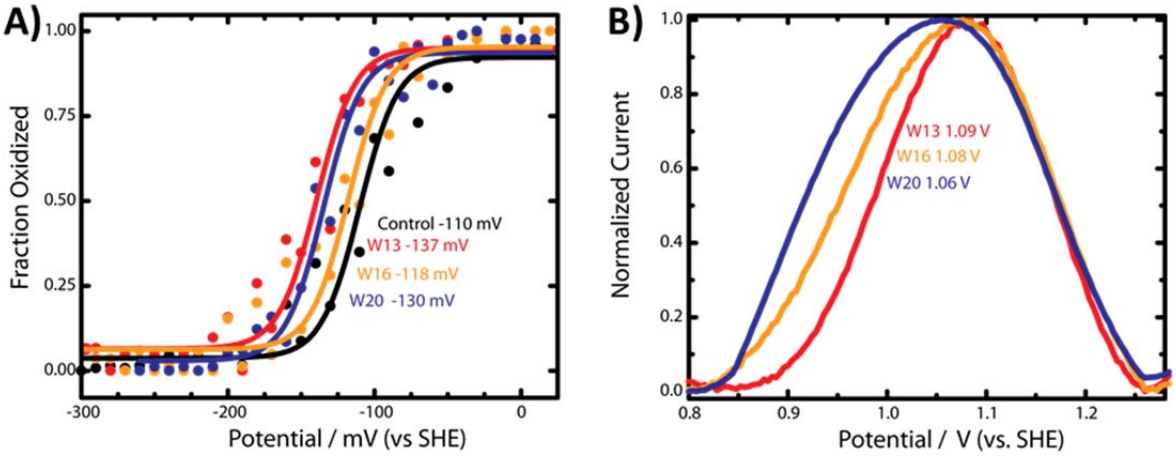

Figure S8. Redox potential of the cofactors. A) Plot of the fraction of reduced maquette calculated from the intensity of the absorption at 475 nm measured during spectro-electrochemical reduction of the flavin. The solid lines show the fit to the data from the Nernst equation for a two-electron reduction. The values of the redox potential can be found in the main text in Table 1. B) The redox potentials of TrpH/TrpH$^{\bullet+}$: W13 1.1 V, W16 1.08 V, and W20 1.06 V.

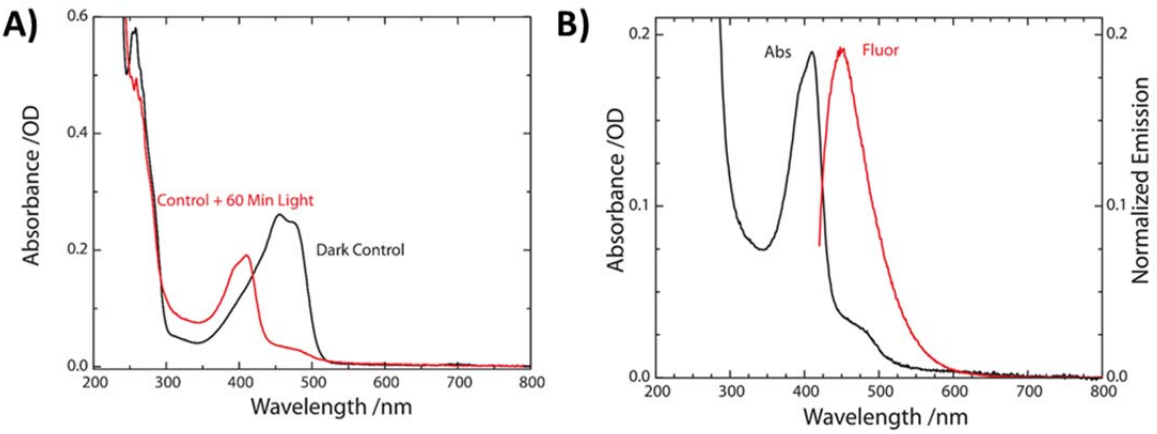

Figure S9. Characterization of the photoproduct. A) Absorption spectra of the control maquette before (black) and after (red) complete photolysis. B) Comparison of the absorption and fluorescence spectra of the photoproduct formed in A. The blue shifts of both the absorbance and fluorescence are consistent with the loss of the ribityl chain of the flavin leading to the formation of lumichrome. These features are blue-shifted relative to the literature for aqueous lumichrome, suggesting that photodegradation does not break the covalent attachment of the flavin to the maquette.

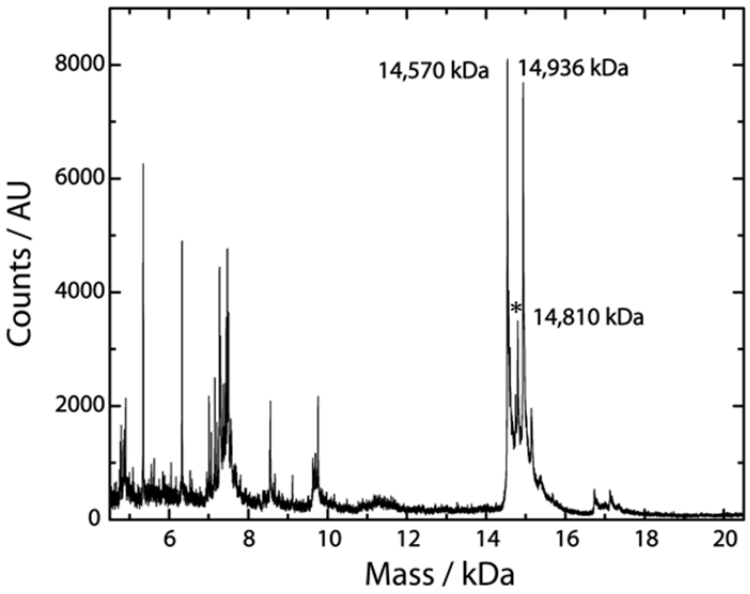

Figure S10. The MALDI-TOF mass spectrum of control maquette after photolysis. A new peak appears at 14810 *m/z* and is marked with an asterisk between the apo- and flavinated maquette signals. The mass difference after photolysis is 125 Da (± 5 Da). This is consistent with the loss of the ribityl chain and the formation of lumichrome.

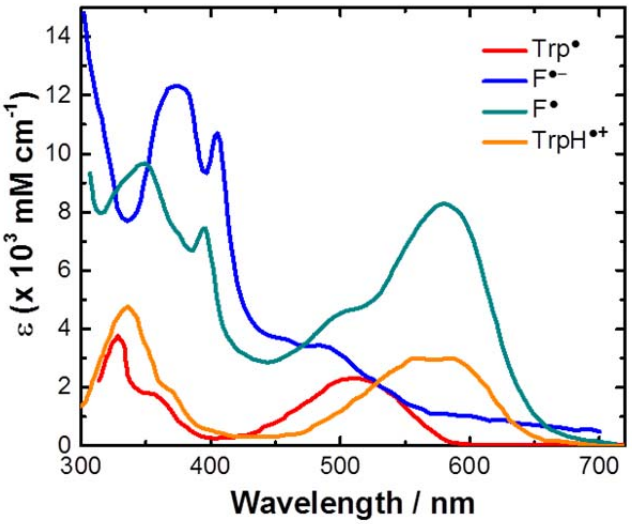

Figure S11. Reference spectra of the various protonation states of the Trp radical (red, orange),[6] and isoelectronic spectra of the flavin radicals expected after covalent attachment of flavin to the maquette: FAD radical anion bound at the 8-position to Cys (blue) from Raibekas *et al.* (2000),[7] and the neutral semiquinone radical of 8-OH-FAD (cyan) from Ghisla *et al*. (1976).[8]

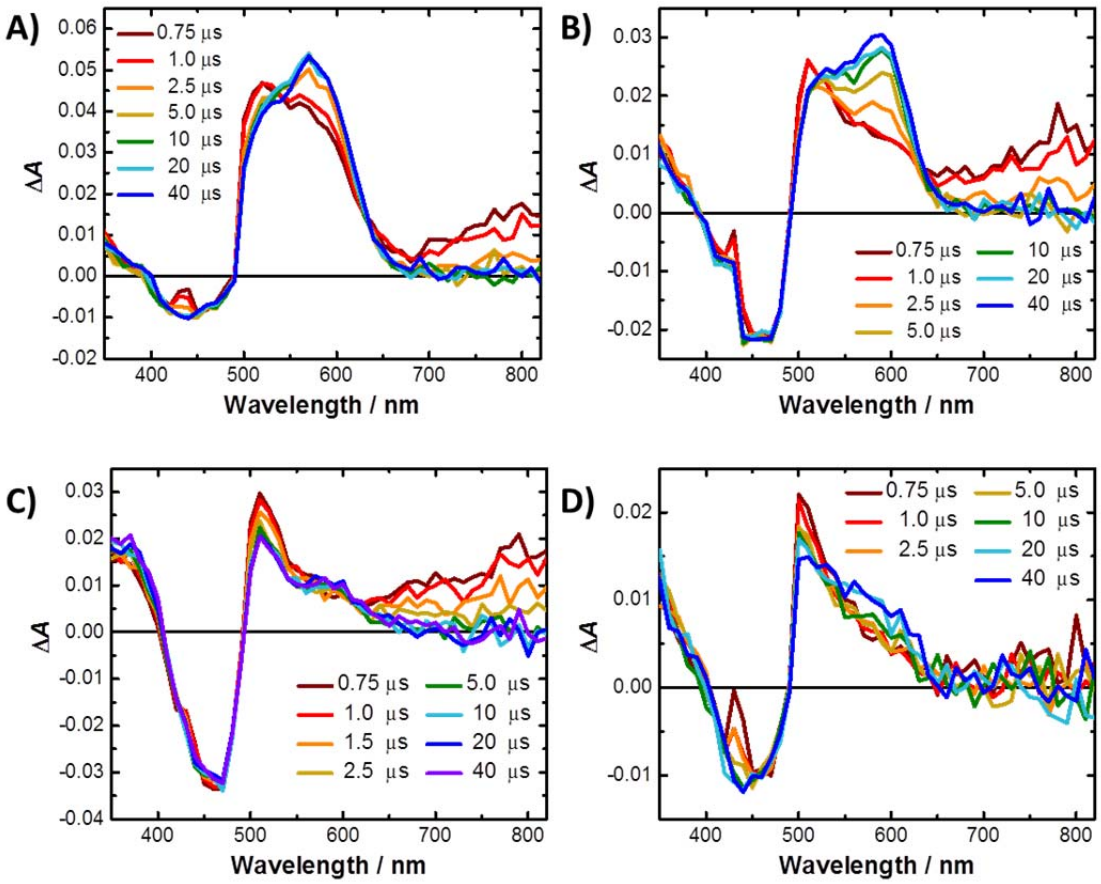

Figure S12. Transient absorption spectra of denatured control maquette (8 M urea) with 10 mM aqueous Trp. The maquette was dissolved in potassium phosphate buffer at pH 4.8 (A), 7.4 (B), and 10.2 (C). Protonation of the flavin radical is observed at low pH, as evidenced by the increase in absorbance at 580 nm. The flavin radical anion absorption dominates the spectrum at pH 10.2. Protonation of the flavin radical is less pronounced when the maquette secondary structure is intact (D, no urea in solution), but a rise in absorbance is still observed at 580 nm consistent with partial protonation to form the neutral flavin semiquinone radical.

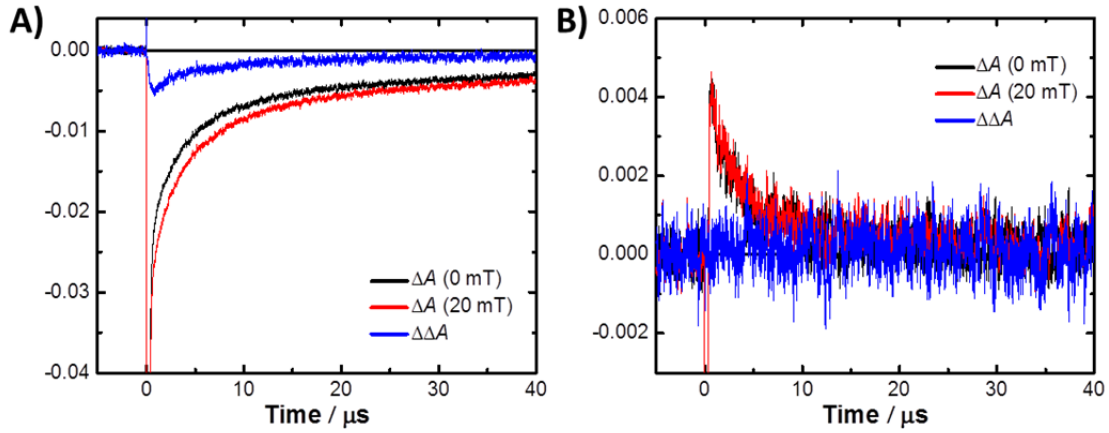

Figure S13. Kinetic traces with field-on (red) field-off (black) and the magnetic field effect (on minus off) for W16 in the region of the ground state bleach at 460 nm (A) and molecular triplet state at 800 nm (B). The absence of any subtraction signal in (B) above the noise confirms that this signal arises from triplet excited state of flavin with no magnetic field effect.

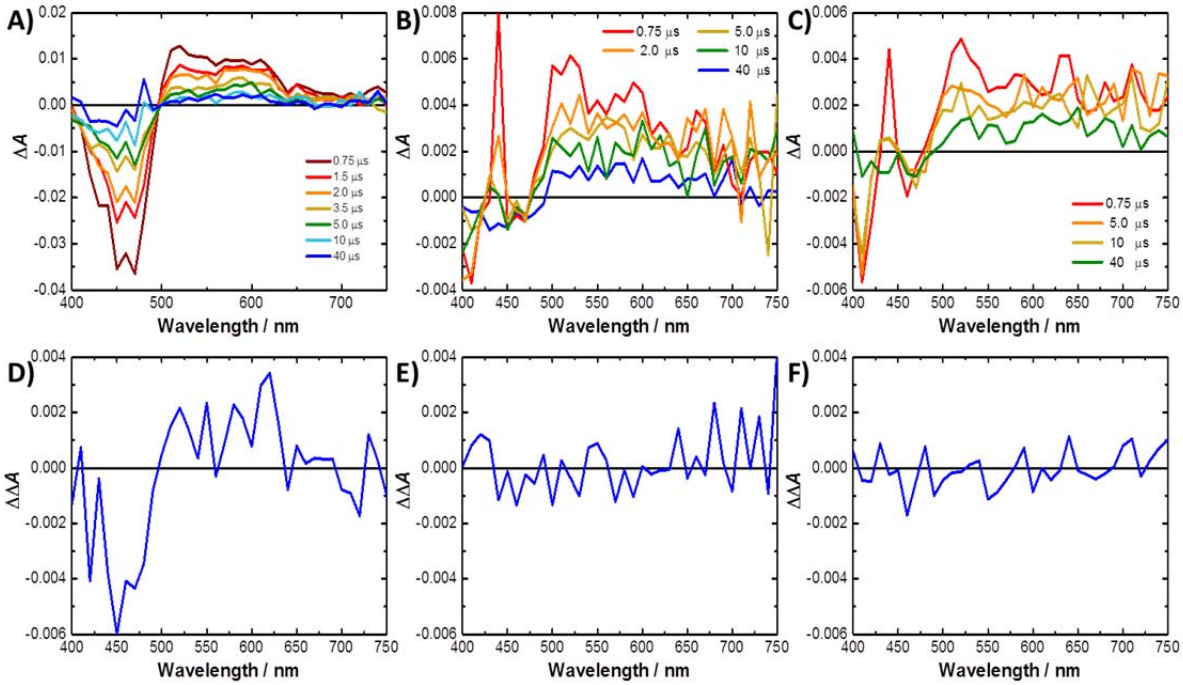

Figure S14. Transient absorption spectra of W13 (A), W20 (B), and the control maquette (C). Action spectra (D, E, F) for the above maquettes averaged over a 1 μs window beginning at 1 μs after photoexcitation. The control TA spectrum (C) shows a broad absorption feature from 500-820 nm and a weak ground state bleach. This is assigned to the molecular triplet excited state of the flavin. W13 (A) shows excited state absorption features similar to those of W16 in Figure 3A. W20 (B) shows broad, weak absorptive features from 500-820 nm, and is largely consistent with the control, although the decay at 520 nm is biexponential, which may indicate that the radical pair is formed in low quantum yield relative to W13 or W16. No MFE effect is measured for the control (F) or W20 (E). For W13, a MFE (D) of approximately 16% of the magnitude of the ESA is observed in W13 between 350-680 nm that mirrors the shape of the excited state absorption in (B).

Table S3: Kinetic analysis of transient absorption data on the single-Trp series of flavomaquettes.

Sample	λ / nm	τ_1 / µs	τ_2 / µs	Constant ($\times 10^3$)
W13	460	0.89	5.79	0.638
W13	520	1.15	6.12	0.634
W13	680-800, averaged	1.15	-	0.294
W16	460	1.71	10.83	0.636
W16	520	1.64	8.86	0.632
W16	800	1.27	-	1.074
W16	680-800, averaged	1.23	-	0.622
W20	520	21.24	1.39	0.705
W20	700	17.01	-	0.569
Control	540-620, averaged	17.24	-	1.007
Control	680-800, averaged	17.18	-	0.618

The kinetic traces were fit to a bi-exponential function with a constant offset for 460 and 520 nm. In the region of the triplet absorption, a single exponential decay was sufficient to fit the data. The value of τ_1 is attributed to decay of any triplet excited state absorption still observable on the timescale of these measurements, and the value of τ_2 is assigned to the decay of the radical absorption, which is marginally faster in W13 relative to W16. For W20, the lifetime of the excited triplet state is substantially longer than in W13 or W16. A shorter lifetime component which is observed in W20 at wavelengths where the radical pair is expected, but the signal intensity is not sufficient to identify the species responsible from the spectrum

References

1. Farid, T. A.; Kodali, G.; Solomon, L. A.; Lichtenstein, B. R.; Sheehan, M. M.; Fry, B. A.; Bialas, C.; Ennist, N. M.; Siedlecki, J. A.; Zhao, Z.; Stetz, M. A.; Valentine, K. G.; Anderson, J. L. R.; Wand, A. J.; Discher, B. M.; Moser, C. C.; Dutton, P. L., Elementary tetrahelical protein design for diverse oxidoreductase functions. *Nat. Chem. Biol.* **2013,** *9* (12), 826-833.
2. Drössler, P.; Holzer, W.; Penzkofer, A.; Hegemann, P., pH dependence of the absorption and emission behaviour of riboflavin in aqueous solution. *Chem. Phys.* **2002,** *282* (3), 429-439.
3. Moser, C. C.; Anderson, J. L. R.; Dutton, P. L., Guidelines for tunneling in enzymes. *Biochim. Biophys. Acta, Bioenerg.* **2010,** *1797* (9), 1573-1586.
4. Henbest, K. B.; Maeda, K.; Hore, P. J.; Joshi, M.; Bacher, A.; Bittl, R.; Weber, S.; Timmel, C. R.; Schleicher, E., Magnetic-field effect on the photoactivation reaction of Escherichia coli DNA photolyase. *Proc. Natl. Acad. Sci. U. S. A.* **2008,** *105* (38), 14395-14399.
5. Ahmad, I.; Fasihullah, Q.; Vaid, F. H. M., Effect of phosphate buffer on photodegradation reactions of riboflavin in aqueous solution. *J. Photochem. Photobiol., B* **2005,** *78* (3), 229-234.
6. (a) Solar, S.; Getoff, N.; Surdhar, P. S.; Armstrong, D. A.; Singh, A., Oxidation of tryptophan and N-methylindole by N3.cntdot., Br2.-, and (SCN)2.- radicals in light- and heavy-water solutions: a pulse radiolysis study. *J. Phys. Chem.* **1991,** *95* (9), 3639-3643; (b) Müller, P.; Bouly, J.-P.; Hitomi, K.; Balland, V.; Getzoff, E. D.; Ritz, T.; Brettel, K., ATP Binding Turns Plant Cryptochrome Into an Efficient Natural Photoswitch. *Scientific Reports* **2014,** *4*, 5175.
7. Raibekas, A. A.; Fukui, K.; Massey, V., Design and properties of human d-amino acid oxidase with covalently attached flavin. *Proc. Natl. Acad. Sci. U. S. A.* **2000,** *97* (7), 3089-3093.

8. Ghisla, S.; Mayhew, S. G., Identification and Properties of 8-Hydroxyflavin -Adenine Dinucleotide in Electron-Transferring Flavoprotein from Peptostreptococcus elsdenii. *Eur. J. Biochem.* **1976,** *63* (2), 373-390.